Experimental and Theoretical Studies on the Reaction of H₂ with NiO: Role of O Vacancies and Mechanism for Oxide Reduction

José A. Rodriguez,*,† Jonathan C. Hanson,† Anatoly I. Frenkel,‡ Jae Y. Kim,† and Manuel Pérez§

Contribution from the Department of Chemistry, Brookhaven National Laboratory, Upton, New York 11973, Department of Physics, Yeshiva University, 245 Lexington Avenue, New York City, New York 10016, and Facultad de Ciencias, Universidad Central de Venezuela, Caracas 1020-A, Venezuela

Received September 4, 2001

Abstract: Reduction of an oxide in hydrogen is a method frequently employed in the preparation of active catalysts and electronic devices. Synchrotron-based time-resolved X-ray diffraction (XRD), X-ray absorption fine structure (NEXAFS/EXAFS), photoemission, and first-principles density-functional (DF) slab calculations were used to study the reaction of H₂ with nickel oxide. In experiments with a NiO(100) crystal and NiO powders, oxide reduction is observed at atmospheric pressures and elevated temperatures (250−350 °C), but only after an induction period. The results of in situ time-resolved XRD and NEXAFS/EXAFS show a direct NiO→Ni transformation without accumulation of any intermediate phase. During the induction period, surface defect sites are created that provide a high efficiency for the dissociation of H₂. A perfect NiO(100) surface, the most common face of nickel oxide, exhibits a negligible reactivity toward H₂. The presence of O vacancies leads to an increase in the adsorption energy of H₂ and substantially lowers the energy barrier associated with the cleavage of the H−H bond. At the same time, adsorbed hydrogen can induce the migration of O vacancies from the bulk to the surface of the oxide. A correlation is observed between the concentration of vacancies in the NiO lattice and the rate of oxide reduction. These results illustrate the complex role played by O vacancies in the mechanism for reduction of an oxide. The kinetic models frequently used to explain the existence of an induction time during the reduction process can be important, but a more relevant aspect is the initial production of active sites for the rapid dissociation of H₂.

I. Introduction

Metal oxides are used as catalysts in a large variety of commercial processes for the conversion of hydrocarbons.[1,2] Selective oxidation, ammoxidation, and selective dehydrogenation probably constitute the most important catalytic applications of metal oxides.[2] In addition, due to their low cost, metal oxides are also used as supports of many other catalytic materials (metals, sulfides, carbides, nitrides, etc).[1,2] In most cases, pure stoichiometric oxides do not exhibit high catalytic activity.[2] One method frequently employed for the preparation of active oxide catalysts involves partial reduction under hydrogen at elevated temperatures.[3−5] In general terms, two different kinetic models have been proposed for the reduction of oxides:[3,5,6] the "nucleation model" and the "interface-controlled model". In the

"nucleation (N) model", the generation of small aggregates or clusters of the new phase (i.e., the reduced oxide) is the rate-determining step. According to this model, there are two main characteristics in the kinetics for oxide reduction: the existence of an induction period and the possibility for autocatalysis.[5,6b] In the "interface-controlled (IC) model", the rapid formation of a uniform layer of the reduced oxide takes place.[3,6] A continuous reduced-phase/oxide interface entirely covers the solid reactant, and the rate of oxide reduction is proportional to the area of such an interface.[3,5,6] In the IC model, the fraction of reduced oxide increases in a nonlinear fashion as a function of time, without the presence of an induction time or substantial autocatalysis.[5] The molecular or atomic processes responsible for these two kinetics models are poorly understood in most situations.[7]

Among the transition-metal oxides, the reduction of NiO by hydrogen has been the object of the most extensive fundamental studies,[3−5,7−10] becoming an important reference system in this topic.[3,5] Nickel oxide appears as a component in many oxidation

* Corresponding author. Fax: 631-344-5815. E-mail: rodrigez@bnl.gov.
† Brookhaven National Laboratory.
‡ Yeshiva University.
§ Universidad Central de Venezuela.
(1) Thomas, J. M.; Thomas, W. J. *Principles and Practice of Heterogeneous Catalysis*; VCH: New York, 1997.
(2) Kung, H. H. *Transition Metal Oxides: Surface Chemistry and Catalysis*; Elsevier: New York, 1989.
(3) Delmon, B. In *Handbook of Heterogeneous Catalysis*; Ertl, G., Knözinger, H., Weitkamp, J., Eds.; Wiley-VCH: New York, 1997; pp 264−277.
(4) Furstenau, R. P.; McDougall, G.; Langell, M. A. *Surf. Sci.* **1985**, *150*, 55.
(5) See Chapter 6 in ref 2.

(6) (a) Delmon, B. *Introduction á la cinétique hétérogène;* Technip: Paris, 1969; Chapter 11. (b) Scholz, J. J.; Langell, M. A. *Surf. Sci.* **1985**, *164*, 543.
(7) Henrich, V. E.; Cox, P. A. *The Surface Science of Metal Oxides*; Cambridge University Press: Cambridge, U.K., 1994.

catalysts[11] and, in addition, is able to catalyze the methanation of CO and the dissociation of N_2O.[1,2,12] At the same time, NiO is a magnetic insulator with well-known electronic properties.[13,14] Thus, the reduction of this material is interesting not only due to its catalytic properties, but also because of possible applications in the fabrication of electromagnetic devices.[13,15] Bulk nickel oxide adopts a cubic rock-salt structure,[13] and the nonpolar (100) plane is the most stable surface.[7,16] Experiments for the reaction of a NiO(100) crystal with hydrogen at 150−350 °C under high-vacuum conditions (1.0×10^{-7}−1.3×10^{-6} Torr) indicate that an induction period precedes the reduction reaction.[4] In contrast, results of H_2 temperature-programmed reduction (>1 Torr H_2 pressure) for bulk powders of NiO and NiO/SiO_2 catalysts show reaction of the oxide only at higher temperatures (400−600 °C),[3,10] and in *many* reduction experiments there is no induction period.[3,8] These differences in behavior could be a consequence of variations in the experimental conditions (the so-called "pressure gap" [17]) or in the morphology of the oxide samples. To clarify these issues, one needs to study the reduction of NiO in situ under atmospheric pressures.

Investigations at Brookhaven National Laboratory have established the feasibility of conducting subminute, time-resolved X-ray diffraction (XRD) experiments under a wide variety of temperature and pressure conditions (−190 °C < *T* < 900 °C; *P* ≤ 45 atm).[18] This important advance results from combining the high intensity of synchrotron radiation with new parallel data-collection devices.[18] Using this unique approach together with near-edge and extended X-ray absorption fine structure (NEXAFS/EXAFS),[19] we monitored the structural changes and reaction kinetics associated with the reduction of NiO powders at moderate or elevated hydrogen pressures. In addition, photoemission[20] and first-principles density functional (DF) slab calculations[21] were used to study the interaction of H_2 with stoichiometric and defect-rich NiO(100) surfaces. Our results illustrate the complexity of the interactions between H_2 and O vacancies during the reduction of an oxide. The O vacancies play a key role in the dissociation of H_2, but only NiO and Ni coexist (i.e., no intermediate NiO_x phase) in the reduction process. In general, the reduction mechanism derived from experiments under high-vacuum conditions can explain the behavior seen under atmospheric pressures.

(8) (a) Houalla, M.; Delannay, F.; Matsuura, I.; Delmon, B. *J. Chem. Soc., Faraday Trans. 1* **1980**, *76*, 2128. (b) Chen, J. G.; Fischer, D. A.; Hardenbergh, J. H.; Hall, R. B. *Surf. Sci.* **1992**, *279*, 13. (c) de Bokx, P. K.; Labohm, F.; Gijzeman, O. L. J.; Bootsma, G. A.; Geus, J. W. *Appl. Surf. Sci.* **1980**, *5*, 321.
(9) Montes, M.; Penneman, Ch.; Hodne, B. K.; Delannay, F.; Grange, P.; Delmon, B. *Appl. Catal.* **1984**, *1*, 309.
(10) Brito, J. L.; Laine, J.; Pratt, K. C. *J. Mater. Sci.* **1989**, *24*, 425.
(11) (a) Choudhary, V. R.; Rajput, A. M.; Mamman, A. S. *J. Catal.* **1998**, *178*, 576. (b) Stone, F. S.; Trevethan, M. A. *Stud. Surf. Sci. Catal.* **1979**, *3*, 417.
(12) Xu, B.; Dong, L.; Fan, Y.; Chen, Y. *J. Catal.* **2000**, *193*, 88.
(13) Hüfner, S. *Adv. Phys.* **1994**, *43*, 183.
(14) Towler, M. D.; Allan, N. L.; Harrison, N. M.; Saunders, V. R.; Mackrodt, W. C.; Aprà, E. *Phys. Rev. B* **1994**, *50*, 5041.
(15) Noguera, C.; Mackrodt, W. C. *J. Phys.: Condens. Matter.* **2000**, *12*, 2163.
(16) (a) Yan, M.; Chen, S. P.; Mitchell, T. E.; Gay, D. H.; Vyas, S.; Grimes, R. W. *Philos. Mag. A* **1995**, *72*, 121. (b) Tasker, P. W.; Duffy, D. M. *Surf. Sci.* **1984**, *137*, 91.
(17) (a) Campbell, C. T. *Adv. Catal.* **1989**, *36*, 1. (b) Rodriguez, J. A.; Goodman, D. W. *Surf. Sci. Rep.* **1991**, *14*, 1.
(18) Norby, P.; Hanson, J. *Catal. Today* **1998**, *39*, 301 and references therein.
(19) (a) Koningsberger, D. C., Prins, R., Eds; *X-ray Absorption: Principles, Applications, Techniques of EXAFS, SEXAFS, and XANES*; Wiley: New York, 1988. (b) Stern, E. A.; Kim, K. *Phys. Rev. B* **1991**, *23*, 3781.
(20) Rodriguez, J. A.; Jirsak, T.; Pérez, M.; González, L.; Maiti, A. *J. Chem. Phys.* **2001**, *114*, 4186.
(21) Payne, M. C.; Allan, D. C.; Arias, T. A.; Johannopoulous, J. D. *Rev. Mod. Phys.* **1992**, *64*, 1045.

II. Experimental and Theoretical Methods

II.1. Photoemission Experiments. The photoemission experiments for the reaction of H_2 with NiO(100) were performed in a standard ultra-high-vacuum system (base pressure ∼2×10^{-10} Torr) with instrumentation for X-ray photoelectron spectroscopy (XPS), Auger electron spectroscopy (AES), low-energy electron diffraction (LEED), and thermal desorption mass spectroscopy (TDS).[20] The XPS spectra were taken employing Al or Mg Kα radiation. Attached to the ultra-high-vacuum (UHV) system was a reaction cell[17a] that was used to expose NiO(100) surfaces to subatmospheric pressures of hydrogen. In a typical experiment, the NiO(100) sample was initially cleaned and characterized in the UHV system and subsequently transferred into the reaction cell, where it was exposed to a mixture of H_2 (5 Torr, 99.9999% purity) and He (95 Torr, 99.9999% purity) at 300−380 °C for a given amount of time. The gases were then pumped out, and the sample was moved back into the UHV system for surface characterization.

The data in section III.1 were collected using a NiO(100) single crystal or NiO(100) films grown on a Ni(100) substrate as described in ref 22. The clean NiO(100) and Ni(100) surfaces were prepared by following procedures reported in the literature.[22,23] Special care was taken in order to ensure that the surface of the NiO(100) crystal contained a minimum amount of defect sites.[23]

II.2. Time-Resolved XRD Experiments. The time-resolved diffraction data were collected on beam line X7B of the National Synchrotron Light Source (NSLS).[18,24] The powder of NiO was acquired from a commercial source (99.998% purity) and exhibited XPS and NEXAFS spectra typical for this oxide.[4,25,26] Samples of NiO were loaded in an open sapphire capillary that was attached to a flow-reaction cell similar to those described in refs 27 and 28. The capillary was connected to $^1/_{16}$-in. Swagelok style fittings with Vespel ferrules. A 0.010-in. chromel−alumel thermocouple was inserted straight into the capillary near the oxide sample.[27] The oxide sample was heated using a small resistance heater wrapped around the capillary. Diffraction patterns were recorded at temperatures in the range of 250−320 °C under a 5% H_2/95% He gas mixture (flow rate = 5−15 cm³/min) using an MAR345 detector. The typical time required for collecting an individual diffraction pattern was in the range of 0.5−2 min. The powder rings were integrated using the FIT2D code.[29] Rietveld refinements were performed with the program GSAS[30] in a manner similar to that followed in a previous work.[31,32]

II.3. Time-Resolved NEXAFS/EXAFS Experiments. All X-ray absorption data were measured in the transmission mode at beamline X16C at the NSLS. The intensity of the incident beam was measured with a 15-cm-long ion chamber filled with air. A 30-cm-long ion chamber was filled with a 50% Ar/50% He mixture and placed after the sample (collinear with the beam direction) to measure the transmitted
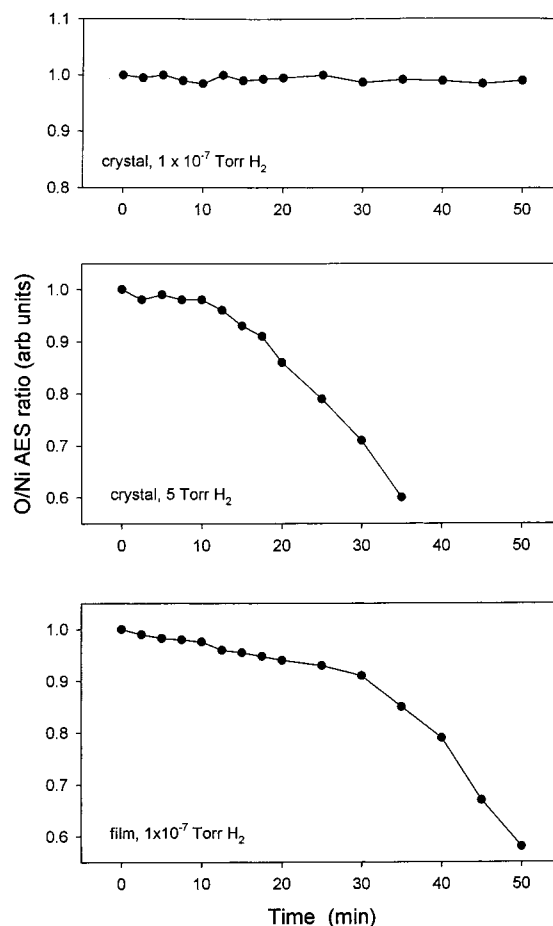
(22) Cappus, D.; Xu, C.; Ehrlich, D.; Dillmann, B.; Ventrice, C. A.; Al-Shamery, K.; Kuhlenbeck, H.; Freund, H.-J. *Chem. Phys.* **1993**, *177*, 533.
(23) (a) Freund, H.-J. *Faraday Discuss.* **1999**, *114*, 1. (b) Wichtendahl, R.; Rodriguez-Rodrigo, M.; Härtel, U.; Kuhlenbeck, H.; Freund, H.-J. *Phys. Stat. Sol. A* **1999**, *173*, 93.
(24) Hastings, J. B.; Suortii, P.; Thomsolin, P.; Kvick, A.; Koetzle, T. *Nucl. Instrum. Methods* **1983**, *208*, 55.
(25) Wagner, C. D.; Riggs, W. M.; Davis, L. E.; Moulder, J. F.; Muilenberg, G. E. *Handbook of X-ray Photoelectron Spectroscopy*; Perkin-Elmer: Eden Praire, MN, 1978; p 80.
(26) (a) Chen, J. G. *Surf. Sci. Rep.* **1997**, *30*, 1. (b) Chen, J. G.; Frühberger, B.; Colaianni, M. L. *J. Vac. Sci. Technol. A* **1996**, *14*, 1668.
(27) Chupas, P. J.; Ciraolo, M. F.; Hanson, J. C.; Grey, C. P. *J. Am. Chem. Soc.* **2001**, *123*, 1694.
(28) Clausen, B. S.; Steffensen, G.; Fabius, B.; Villadsen, J.; Freidenhans, R.; Topsøe, H. *J. Catal.* **1991**, *132*, 524.
(29) Hammersely, A. P.; Svensson, S. O.; Thompson, A. *Nucl. Instrum. Methods Phys. Res.* **1994**, *346*, 321.
(30) Larson, A. C.; von Dreele, R. B. *GSAS General Structure Analysis System*, Report LAUR 86-748; Los Alamos National Laboratory: Los Alamos, NM, 1995.
(31) Norby, P.; Pashni, F. I.; Gualtieri, A. F.; Hanson, J. C.; Grey, C. P. *J. Phys. Chem. B* **1998**, *102*, 839.
(32) Rodriguez, J. A.; Hanson, J. C.; Chaturvedi, S.; Maiti, A.; Brito, J. L. *J. Phys. Chem. B* **2000**, *104*, 8145.

beam intensity. A thin sample of Ni metal foil was used to calibrate the X-ray energy during each scan. The calibration measurements were made with another 30-cm-long Ar-filled ion chamber placed after the standard Ni foil.

For the time-resolved NEXAFS/EXAFS measurements at three different reduction temperatures (260, 280, and 300 °C), we prepared samples from the same commercially obtained NiO powder used in our XRD measurements, by spreading it with a brush over adhesive Kapton polyamide tape. Kapton is relatively transparent for X-rays at the 8 keV energy range, does not decompose at temperatures up to 400 °C, and thus makes a good support. The absorption edge steps were ca. 0.2–0.3 at the Ni *K* absorption edge (8333 eV) in all the samples studied, ensuring that the thickness effects in X-ray absorption data[19] were avoided. The samples were then loaded into a custom-designed and custom-built cell that allows simultaneous in situ X-ray fluorescence and transmission measurements over an operating temperature range of −120 to 500 °C. The present experimental setup is almost the same as that used in the previous in situ structural studies, at the same beam line, for Pt nanoparticles reduction with H_2.[33–35] The samples were exposed to a flow of pure H_2 (∼50 cm³/min), while the NEXAFS or EXAFS measurements were taken repetitiously during reaction at 260, 280, or 300 °C. The temperature was monitored with a chromel/alumel thermocouple mounted directly on the sample stage. With a suitable combination of energy scan parameters, the duration of each NEXAFS scan was ∼4 min. In the case of the EXAFS measurements, due to the longer energy range (up to 1000 eV above the edge), the repetition time was ∼20 min. Since the reduction reaction was fast at 300 and 280 °C, EXAFS data were collected only at 260 °C.

II.4. Theoretical Methods. The first-principles density functional (DF) calculations reported in section III.1 were performed using the CASTEP (Cambridge Serial Total Energy Package) suite of programs.[21,36] In this code, the Kohn–Sham implementation of DF theory is used to obtain the total energy of the system. CASTEP has an excellent track record in accurate prediction of geometry and energetics for oxide systems.[20,37–42] In this code, the wave functions of valence electrons are expanded in a plane wave basis set with k-vectors within a specified energy cutoff E_{cut}. Tightly bound core electrons are represented by nonlocal ultrasoft pseudopotentials.[43] Brillouin zone integration is approximated by a sum over special *k*-points chosen using the Monkhorst–Pack scheme.[44] In all the calculations, the kinetic energy cutoff E_{cut} and the density of the Monkhorst–Pack *k*-point mesh were chosen high enough in order to ensure convergence of the computed structures and energetics. The exchange-correlation contribution to the total electronic energy is treated in a spin-polarized generalized-gradient-corrected (GGA) form of the local density approximation (LDA).[45] Since the DF calculations were performed at the GGA level, one can expect reasonable predictions for the bonding energies of the H_2 molecule on NiO and NiO_{1-x}.[38,42,45,46] In any case, in this work our main interest is in qualitative trends in the energetics, and not in absolute

(33) Nashner, M. S.; Frenkel, A. I.; Shapley, J. R.; Nuzzo, R. G. *J. Am. Chem. Soc.* **1997**, *119*, 7760.
(34) Nashner, M. S.; Frenkel, A. I.; Sommerville, D.; Hills, C. W.; Shapley, J. R.; Nuzzo, R. G. *J. Am. Chem. Soc.* **1998**, *120*, 8093.
(35) Hills, C. W.; Nashner, M. S.; Frenkel, A. I.; Shapley, J. R.; Nuzzo, R. G. *Langmuir* **1999**, *15*, 690.
(36) Milman, V.; Winkler, B.; White, J. A.; Pickard, C. J.; Payne, M. C.; Akhmatskaya, E. V.; Nobes, R. H. *Int. J. Quantum Chem.* **2000**, *77*, 895.
(37) Rodriguez, J. A.; Jirsak, T.; Sambasivan, S.; Fischer, D.; Maiti, A. *J. Chem. Phys.* **2000**, *112*, 9929.
(38) (a) Sorescu, D. C.; Rusu, C. N.; Yates, J. T. *J. Phys. Chem. B* **2000**, *104*, 4408. (b) Sorescu, D. C.; Yates, J. T. *J. Phys. Chem. B* **1998**, *102*, 4556.
(39) Rodriguez, J. A.; Maiti, A. *J. Phys. Chem. B* **2000**, *104*, 3630.
(40) Refson, K.; Wogelius, R. A.; Fraser, D. G.; Payne, M. C.; Lee, M. H.; Milman, V. *Phys. Rev. B* **1995**, *52*, 10823.
(41) Rodriguez, J. A.; Jirsak, T.; Pérez, M.; Chaturvedi, S.; Kuhn, M.; González, L.; Maiti, A. *J. Am. Chem. Soc.* **2000**, *122*, 12362.
(42) Rodriguez, J. A. *Theor. Chem. Acc.*, in press.
(43) Vanderbilt, D. *Phys. Rev. B* **1990**, *41*, 7892.
(44) Monkhorst, H. J.; Pack, J. D. *Phys. Rev. B* **1976**, *13*, 5188.
(45) White, J. A.; Bird, D. M. *Phys. Rev. B* **1994**, *50*, 4954.
(46) (a) Ziegler, T. *Chem. Rev.* **1991**, *91*, 651. (b) van Santen, R. A.; Neurock, M. *Catal. Rev.-Sci. Eng.* **1995**, *37*, 557.

Figure 1. O/Ni Auger ratio for a NiO(100) crystal (top and center) and a NiO(100) film (bottom) exposed to different pressures of molecular hydrogen at 350 °C.

values. The structural parameters of the $H_2/NiO(100)$ and H_2/NiO_{1-x}-(100) systems in their different configurations were determined using the Broyden–Fletcher–Goldfarb–Shanno (BFGS) minimization technique, with the following thresholds for the converged structures: energy change per atom less than 5×10^{-6} eV, residual force less than 0.02 eV/Å, and the displacement of atoms during the geometry optimization less than 0.001 Å. For each optimized structure, the partial charges on the atoms were estimated by projecting the occupied one-electron eigenstates onto a localized basis set with a subsequent Mulliken population analysis.[47,48] Mulliken charges have well-known limitations[49] but are nevertheless useful as a qualitative tool.

III. Results

III.1. Reaction of H_2 with NiO(100): Photoemission and DF Studies. The top and center panels in Figure 1 show AES data for the interaction of a NiO(100) crystal with hydrogen under high vacuum (1×10^{-7} Torr of H_2, in UHV chamber) and moderate (5 Torr of H_2/95 Torr of He, in reaction cell) pressures at 350 °C. In the *Y* axis is plotted the normalized ratio of the O KL_2L_2 and Ni $L_3M_{4,5}M_{4,5}$ Auger signals for the oxide substrate.[4] Initially, the surface of the NiO(100) crystal exhibited a minimum amount of defect sites. In test experiments, NO-

(47) Segall, M. D.; Pickard, C. J.; Shah, R.; Payne, M. C. *Phys. Rev. B* **1996**, *54*, 16317.
(48) Segall, M. D.; Pickard, C. J.; Shah, R.; Payne, M. C. *Mol. Phys.* **1996**, *89*, 571.
(49) (a) Szabo, A.; Ostlund, N. S. *Modern Quantum Chemistry*; McGraw-Hill: New York, 1989. (b) Wiberg, K. B.; Rablen, P. R. *J. Comput. Chem.* **1993**, *14*, 1504.

TDS spectra displayed the line shape expected for a NiO(100) surface with a negligible concentration of defects or imperfections.[23] The results of TDS experiments indicated that the NiO-(100) crystal did not adsorb significant coverages of H_2 at 27 or −193 °C. From these experiments, we estimate that the adsorption energy of H_2 on a flat NiO(100) surface is ≤5 kcal/mol. The AES results in the top panel of Figure 1 show no reaction between H_2 and the NiO(100) crystal after 50 min of exposure to the gas at 1×10^{-7} Torr and 350 °C. Longer reaction times (up to 120 min) under these conditions or lower temperatures (27 or 125 °C) did not lead to significant changes in the O/Ni AES ratio. Thus, one can conclude that the probability for the $H_{2,gas} + Ni-O_{sol} \rightarrow H_2O_{gas} + Ni_{sol}$ reaction on a NiO(100) surface is very small ($<10^{-3}$ per H_2 collision). A substantial decrease in the O/Ni AES ratio was observed when the NiO(100) crystal was exposed to 5 Torr of H_2 at 350 °C (center panel in Figure 1) *but only after an induction period of 10−12 min.* The surface produced by this treatment did not have a LEED pattern, and its Ni 2p XPS spectrum showed a large attenuation in the high-binding-energy satellites that are characteristic of NiO.[4,25] After CO was adsorbed on this surface at −193 °C, desorption peaks at −73, 27, and 127 °C were seen in CO-TDS spectra. The peak at 127 °C corresponds to CO desorption from Ni sites that were completely reduced,[50] whereas the peak at −73 °C denotes CO evolution from Ni sites that remained almost fully oxidized.[23,50,51]

The bottom panel in Figure 1 shows AES data for the reaction of H_2 with a NiO(100) film grown on a Ni(100) substrate.[22] It is known that this type of epitaxial films contain a substantial amount of defects and imperfections.[52] Indeed, upon dosing of NO at −193 °C, the corresponding NO-TDS spectra for the film displayed a peak at ∼ −50 °C with a clear shoulder toward higher temperatures, which is characteristic of defects on the oxide surface.[23] By comparing the results for the NiO(100) film and the NiO(100) crystal in Figure 1 (both sets of experiments done at 1×10^{-7} Torr of H_2 and 350 °C), it is obvious that the presence of defects accelerates the reduction rate of the oxide surface. Nevertheless, the data for the NiO(100) film still exhibit an induction time before the reaction rate becomes fast. In experiments with other NiO(100) films, we found that the induction time shortened when the sample temperature was increased to 380 °C or when the H_2 pressure was raised above 1×10^{-7} Torr. For NiO(100) films with a high concentration of defects there is no induction time,[8b] and the kinetics for reduction in H_2 is very different from that of a NiO(100) crystal.

The results in Figure 1 are consistent with previous studies,[4] which showed an induction period in the reduction of NiO-(100) surfaces exposed to low pressures ($\leq 1.3 \times 10^{-6}$ Torr) of H_2. Our data show that *a similar phenomenon can occur under atmospheric pressures*, depending on how well ordered is the oxide surface. The chemical reactivity observed for the NiO-(100) crystal in this work was smaller than that found in ref 4, probably due to the much lower concentration of defects in the surface of our sample.[23] The induction times in the reduction of NiO(100) surfaces have been explained using a kinetic model in which the reduction is controlled both by the rate of removal of lattice oxide at the surface and by the diffusion of subsurface oxygen to the oxygen-depleted surface.[4,6b] From our results and those of others,[8b] we believe that the induction time reflects the need to generate sites on the oxide surface with a high activity for the dissociation of H_2. Without atomic hydrogen on the surface, there cannot be removal of oxygen, and the interactions of H_2 with a flat NiO(100) surface are very weak according to TDS. This is also shown by first-principles DF calculations.

The bonding of H_2 to NiO(100) was studied using a four-layer slab and the supercell approach.[21] Three- or four-layer slabs are frequently used to model the adsorption of small molecules on nonpolar oxide surfaces.[20,38,39,41,42,53] The geometry optimization for bulk NiO gave a rock-salt unit cell with $a = 4.198$ Å. This cell parameter is very close to those obtained in experimental measurements (4.168 Å[54]) and other theoretical calculations (4.19−4.26 Å[7,14,53]). After the geometry optimization of bulk NiO, the (100) face was cleaved, followed by the construction of a three-dimensionally periodic supercell with a vacuum of 12.5 Å on top of the free surface. In the slab calculations, the structural geometry of the first two layers was relaxed, while the other two layers were frozen at the bulk crystalline spacing in order to mimic the presence of a semi-infinite crystalline material beneath the surface. For the clean NiO(100) system, the DF calculations predict that the outermost ion plane relaxes inward by 2−3%. LEED $I-V$ studies reveal a contraction of ∼2%.[55] Calculations based on an electrostatic model[16] also suggest that one can regard the geometry of the (100) surface as a nearly perfect bulk termination.

The H_2 molecule was adsorbed on one face of our slab model, and the geometries of the adlayer and first two layers of the slab were fully relaxed. We examined the bonding of H_2 to Ni or O sites of the oxide surface ($\theta_{H_2} = 0.25$ ML, only one-quarter of the Ni or O sites were covered by H_2) in η^1-H and η^2-H,H configurations. The molecule did not bond to O sites. On the Ni sites, the bonding interactions were very weak, with adsorption energies of 1.9 (η^2-H,H) and 2.3 kcal/mol (η^1-H). Essentially, there was no charge transfer from the cations into the LUMO of H_2 or from the molecule into the surface, and the H−H bond distance (0.75−0.76 Å) remained very similar to that calculated for free H_2 (0.74 Å). We found that the dissociation of the molecule ($H_{2,ads} \rightarrow 2H_{ads}$) was somewhat (1.6 kcal/mol) more favorable on two neighboring Ni atoms (homolytic bond cleavage) than on adjacent Ni and O atoms (heterolytic bond cleavage), but in both cases the breaking of the H−H bond was an uphill process. The less endothermic case is shown in the top of Figure 2. Initially, the H_2 molecule is bound in an η^2-H,H configuration on a Ni site. In the final state, Ni−H bonds have been formed on two neighbor Ni atoms, and the stability of the system has *decreased* by 6.2 kcal/mol. In addition, there is an energy barrier of ∼16 kcal/mol associated with the cleavage of the H−H bond. Clearly, the H_2 molecule should prefer desorption instead of dissociation on a flat NiO-(100) surface. This agrees with the trends seen in the experiments presented above.

Recent theoretical works stress the importance of O vacancies in the chemistry of oxide surfaces.[56,57] Based on this and the

(50) Öfner, H.; Zaera, F. *J. Phys. Chem. B* **1997**, *101*, 9069.
(51) Vesecky, S. M.; Xu, X.; Goodman, D. W. *J. Vac. Sci. Technol. A* **1994**, *12*, 2114.
(52) Sebastian, I.; Bertrams, T.; Meinel, K.; Neddermeyer, H. *Faraday Discuss.* **1999**, *114*, 129.

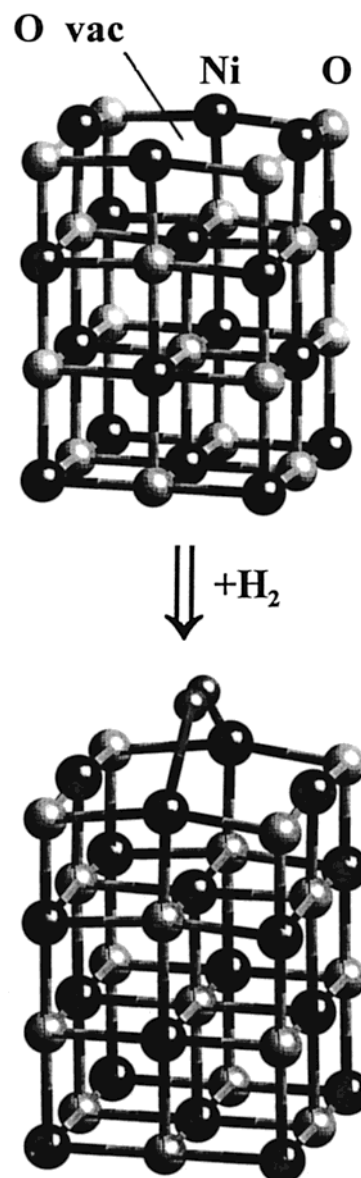(53) Mackrodt, W. C.; Noguera, C.; Allan, N. L. *Faraday Discuss.* **1999**, *114*, 105.
(54) Wyckoff, R. W. G. *Crystal Structures*; Insterscience: New York, 1964.
(55) (a) Netzer, F. P.; Prutton, M. *J. Phys. C* **1975**, *8*, 2401. (b) Kinniburgh, C. G.; Walker, J. A. *Surf. Sci.* **1977**, *63*, 274. (c) Welton-Cook, M. R.; Prutton, M. *J. Phys. C* **1980**, *13*, 3993.
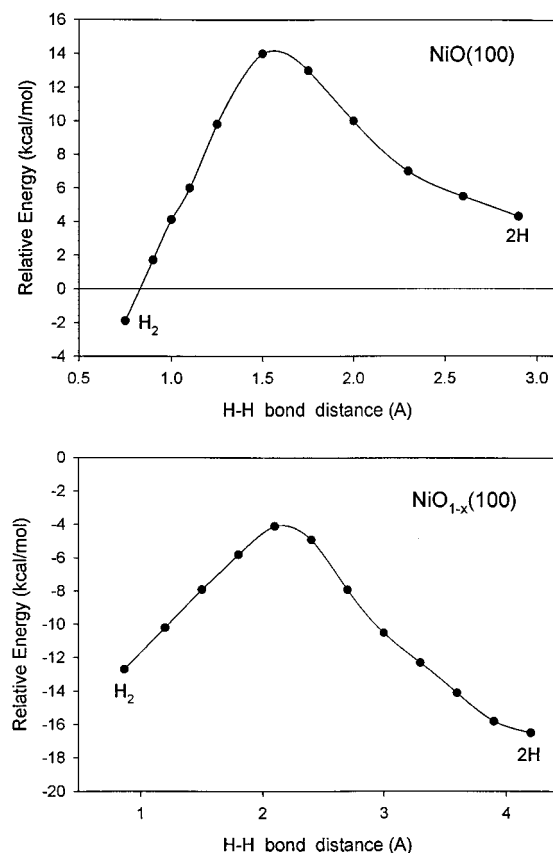
Figure 2. (Top) Calculated (DF-GGA) energy change for the dissociation of H_2 on a flat NiO(100) surface. Initially, the H_2 molecule was bonded to a Ni center in an η^2-H,H configuration. The H—H distance then changed to the indicated values, and all the other surface structural parameters were relaxed. In the final state, one H atom was sitting on a Ni center, while the other H was on a second Ni center. (Bottom) Calculated (DF-GGA) energy change for the dissociation of H_2 near an O vacancy of a $NiO_{1-x}(100)$ surface. Initially, the H_2 molecule was bridging two Ni atoms in an η^2-H,H configuration. The H—H distance then changed to the indicated values, and all the other surface structural parameters were relaxed. In the final state, one H atom was sitting on a Ni center, while the second H was on an adjacent Ni center. In both panels, the reference or "0" of energy corresponds to the sum of the total energies for free H_2 and the corresponding bare slab. Negative values indicate a system with the adsorbate(s) bound to the surface.

data in Figure 1, we decided to study the adsorption of H_2 on a $NiO_{1-x}(100)$ surface. To create a surface with O vacancies, we removed 25% of the oxygens in the first layer of our slab model (see top of Figure 3). Images of scanning tunneling microscopy show that this type of O vacancies exist on NiO-(100),[58] but in many situations they do not adopt the p(2 × 2) periodicity used in our $NiO_{1-x}(100)$ slab model. After relaxing the first two layers of the slab, there were structural changes in the region near a missing oxygen with the adjacent Ni atoms moving downward and sideways (0.05−0.12 Å) to strengthen their bonds with the remaining oxygens. On average, the Ni atoms near an O vacancy displayed a reduction of ∼0.12e in their positive charge. The bottom of Figure 3 displays the most stable configuration found for H_2 on the $NiO_{1-x}(100)$ surface
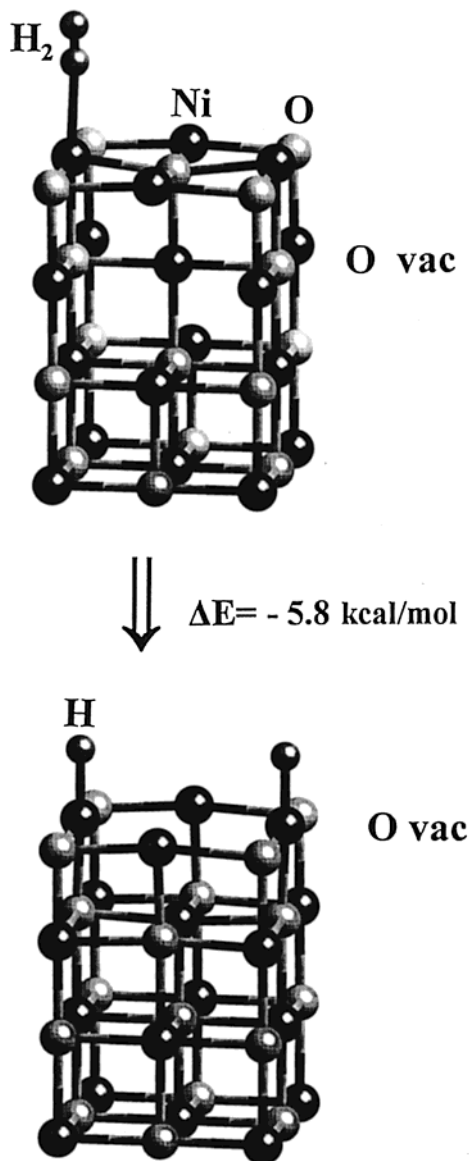
(56) (a) Pacchioni, G. A. *Surf. Rev. Lett.* **2000**, *7*, 277. (b) Pacchioni, G. A.; Pescarmona, P. *Surf. Sci.* **1998**, *412/413*, 657.
(57) Chen, M.; Friend, C. M.; Kaxiras, E. *J. Am. Chem. Soc.* **2001**, *123*, 2224 and references therein.
(58) Castell, M. R.; Wincott, P. L.; Condon, N. G.; Muggelberg, C.; Thornton, G.; Dudarev, S. L.; Sutton, A. P.; Briggs, G. A. D. *Phys. Rev. B* **1997**, *55*, 7859.

Figure 3. Schematic view of the four-layer slabs used to model the $NiO_{1-x}(100)$ and $H_2/NiO_{1-x}(100)$ systems. The Ni and O atoms are represented by dark and gray spheres, respectively. For simplicity, only the Ni and O atoms near an O vacancy are shown. In the first layer of each slab, 25% of the oxygen atoms were missing, as O vacancies.

($\theta_{H_2} = 0.25$ ML). In this configuration, the molecule is bridging two of the Ni atoms located around an O vacancy. Upon geometry optimization, the calculated adsorption energy for the molecule was 12.8 kcal/mol, which is much bigger than the adsorption energies calculated for H_2 on a perfect NiO(100) system. In addition, on $NiO_{1-x}(100)$, the H—H bond length increases to 0.87 Å, facilitating dissociation of the adsorbate. Indeed, the dissociation of H_2 on two Ni sites near an O vacancy is an exothermic process (see bottom of Figure 2). There is an energy barrier of ∼8 kcal/mol for the $H_{2,ads} \rightarrow 2H_{ads}$ reaction; *nevertheless, near an O vacancy the dissociation channel clearly can compete with desorption*, which is not the case on a perfect NiO(100) surface (Figure 2).

The interaction between H_2 and O vacancies can be complex. O vacancies affect the chemistry of H_2 on the oxide surface, and, at the same time, the adsorbate can affect the distribution of O vacancies in the surface and subsurface regions of the

Figure 4. Energy change associated with the migration of O vacancies from the subsurface region to the surface in H$_2$/NiO$_{1-x}$(100). For simplicity, only a few atoms in the slab model are shown. Initially, H$_2$ is adsorbed on a perfect NiO(100) surface (η^2-H,H configuration) with O vacancies in the subsurface region. In the final state, the O vacancies are located at the surface with H$_2$ adsorbed above them.

sample. Using our four-layer slab model, we compared the relative stability of O vacancies on the surface (first layer) and subsurface (second layer) regions of a NiO(100) system. In each case, we removed 25% of the oxygen atoms in the corresponding layer. After full geometry relaxation, we found that the system with the oxygen vacancies in the subsurface or bulk was 9.1 kcal/mol more stable than the system with surface vacancies. Thus, a large fraction of the O vacancies in a NiO sample should be away from the surface. But upon interaction with hydrogen, the migration of O vacancies from the bulk to the surface becomes an exothermic process ($\Delta E = -5.8$ kcal/mol, Figure 4). Such a migration probably occurs in the induction period during the reduction of NiO samples. It can lead to autocatalysis: the rate of vacancy migration depends on the lattice strain, which reflects the degree of reaction and structural heterogeneity of the system.
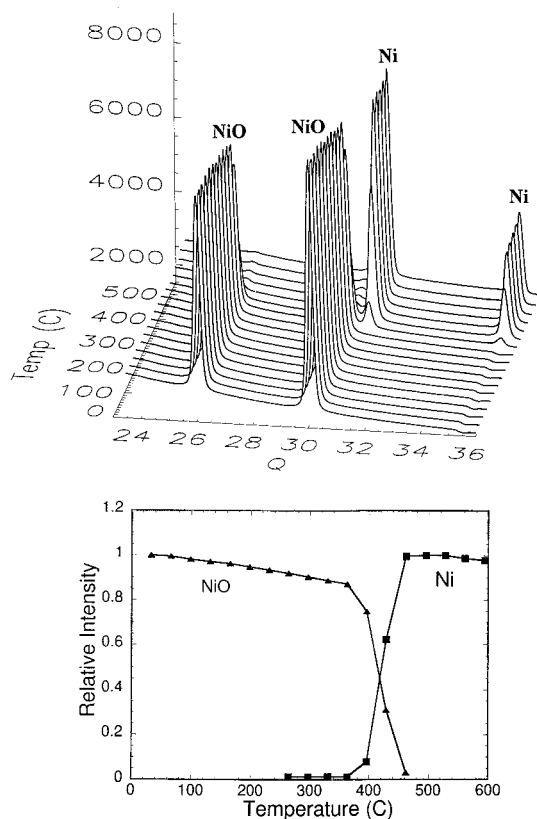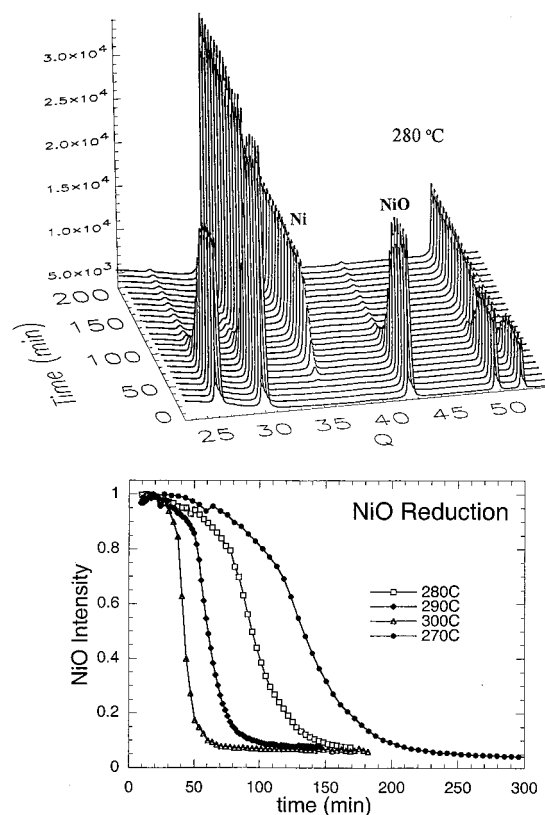

Figure 5. (Top) Time-resolved X-ray diffraction patterns acquired during the heating (20 °C/min) of a NiO powder from 25 to 600 °C under a flow (15 cm^3/min) of 5% H$_2$/95% He. Q is in inverse nanometer units. (Bottom) Integrated intensity for diffraction lines of NiO and Ni as a function of sample temperature.

From our results, it is clear that the generation of surface defects should affect the magnitude of the induction period. The interplay between the removal of oxygen at the surface and bulk, as proposed in refs 4 and 6b, can be important, but a more relevant aspect is the initial production of active sites for the rapid dissociation of H$_2$. This alone can explain the autocatalytic nature of the reduction process. Once a large coverage of H is available on the surface, then the efficient removal of O from the bulk[4,6b] or nucleation of the new Ni phase[3,5] can become rate-limiting factors.

III.2. Reaction of H$_2$ with NiO Powders: Time-Resolved XRD Studies. Due to its high stability, the (100) plane is the most common face in bulk polycrystalline powders of nickel oxide.[7,16] On the basis of this, one could expect that the chemistry seen in the previous section for the NiO(100) surfaces would be reflected in the behavior of NiO powders. However, results of H$_2$ temperature-programmed reduction (TPR) for powders of NiO and NiO/SiO$_2$ catalysts show reaction of the oxide only at 400−600 °C,[3,10] and in many reduction experiments there is no induction time.[3,8] This seems to suggest that the mechanism responsible for the reduction of a NiO(100) crystal may not occur or be valid when dealing with polycrystalline samples of NiO. To clarify this issue, we studied the reduction of NiO powders in situ under atmospheric pressures using time-resolved XRD and NEXAFS/EXAFS.
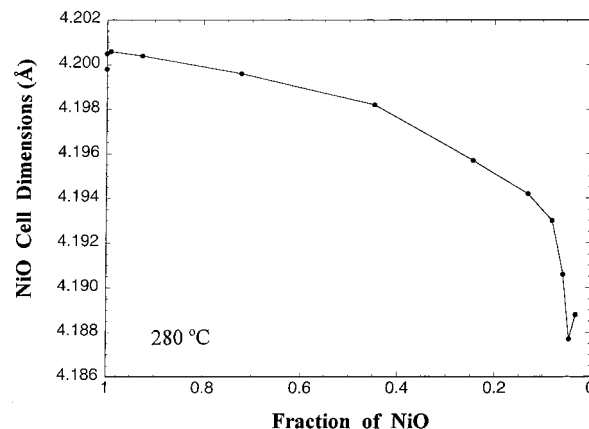
Figure 5 shows diffraction patterns obtained during the temperature-programmed reduction of a NiO powder. The sample was in a flow reactor (15 cm^3 min^{-1}, 5% H$_2$/95% He), and the XRD data were recorded while the temperature was

Figure 6. (Top) Time-resolved X-ray diffraction patterns for the isothermal reduction of a NiO powder at 280 °C under a flow (15 cm³/min) of 5% H₂/95% He. *Q* is in inverse nanometer units. (Bottom) Integrated intensity for diffraction lines of NiO as a function of time during isothermal reductions at 270, 280, 290, and 300 °C.

ramped from 25 to 600 °C at a rate of 20 °C/min. Typical conditions for H₂-TPR experiments were used.[10] Initially, one sees only the typical diffraction lines for NiO.[59] There is a small decrease in the intensity of these lines up to ~360 °C, where a large intensity drop occurs and simultaneously diffraction lines for metallic Ni[60] appear. *A direct NiO→Ni transformation is observed, without any well-ordered intermediate phase.* The oxide reduction essentially occurs between 400 and 460 °C (bottom of Figure 5). This is the temperature range in which consumption of H₂ is observed in several TPR measurements.[3,10] In such experiments, the rapid ramping of the sample temperature makes it very difficult to detect the existence of an induction time and makes the apparent reaction temperature higher.

Figure 6 displays time-resolved XRD data for the reduction of NiO powder under isothermal conditions. The raw data at the top were taken at a constant temperature of 280 °C. During the first 50 min, no major changes are seen in the intensity of the diffraction lines for NiO. The NiO lines then begin to disappear, and simultaneously lines for metallic Ni appear, again without diffraction features for an intermediate suboxide. The bottom of Figure 6 shows how the concentration of NiO powder (determined from the intensity of the NiO diffraction lines) changes as a function of time at 270, 280, 290, and 300 °C. Clearly, *there is an induction period for the reduction of NiO powder,* as was seen for the NiO(100) surfaces. The magnitude

(59) JCPDS Powder Diffraction File No. 4-835, International Centre for Diffraction Data, Swarthmore, PA, 1989.
(60) JCPDS Powder Diffraction File No. 4-580, International Centre for Diffraction Data, Swarthmore, PA, 1989.

Figure 7. NiO cell dimensions for the reduction reaction at 280 °C (15 cm³/min, 5% H₂/95% He).

of the induction time decreases when the temperature of the sample increases. No induction time was found for experiments done at temperatures higher than 310 °C. In principle, the higher the temperature, the easier to create the surface sites with a high efficiency for the dissociation of H₂ and the removal of O from the system. In a series of experiments, we found that the presence of defects or oxygen vacancies in a NiO powder strongly affects the magnitude of the induction time and, in extreme cases (i.e., highly defective samples), can suppress it. A quantitative comparison of the experiments in Figures 1 and 6 is impossible due to the different techniques used, but it was obvious that it was much more difficult to reduce the NiO(100) systems than NiO powder. For example, under nearly atmospheric pressures, no induction time was observed for the NiO powder at temperatures above 310 °C, whereas one was seen for the NiO-(100) crystal at 350 °C (Figure 1). As discussed above, the very low concentration of defects in the NiO(100) crystal made this sample relatively unreactive for the dissociation of H₂.

Figure 7 shows the variation in the NiO cell dimensions for the reduction at 280 °C in Figure 6. The cell parameters were obtained through Reitveld refinement of the XRD patterns with the GSAS program.[30] As the reduction reaction proceeds, there is a significant contraction in the cell dimensions of NiO. This results from the formation of O vacancies within the NiO lattice.[18,58] *Initially, the bigger the contraction of the NiO cell, the larger the number of O vacancies, and the faster the rates of H₂ dissociation and reduction of the oxide.* This is consistent with the DF results in Figure 2, and stresses the important role played by O vacancies in the reduction process. Toward the end (fraction of NiO <0.2), the H coverage on the surface of the system is large, and phenomena like the removal of O from the bulk[4,6b] or nucleation of the Ni phase[3,5] are probably rate limiting.

III.3. Reaction of H₂ with NiO Powders: Time-Resolved NEXAFS/EXAFS Studies. Partially reduced intermediates or suboxides can be produced during the reduction of oxide compounds.[2,61] The time-resolved XRD data show a direct NiO→Ni transformation without a well-ordered intermediate phase. This does not rule out the possible existence of an amorphous NiO_x phase. In fact, it could be argued that the induction time in Figure 6 is associated with the formation of

(61) Ressler, T.; Jentoft, R. E.; Wienold, J.; Gunter, M. M.; Timpe, O. *J. Phys. Chem. B* **2000**, *104*, 6360.

Table 1. Coordination Numbers (*N*) and Nearest-Neighbor Distances (*R*, in Å) in Ni and NiO[a]
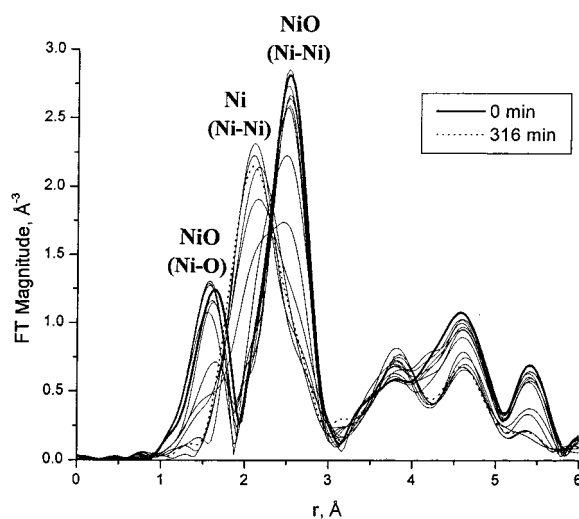
	Ni–O		Ni–Ni	
	N	R	N	R
NiO	6	2.08	12	2.95
Ni			12	2.49

[a] From refs 54, 59, and 60.
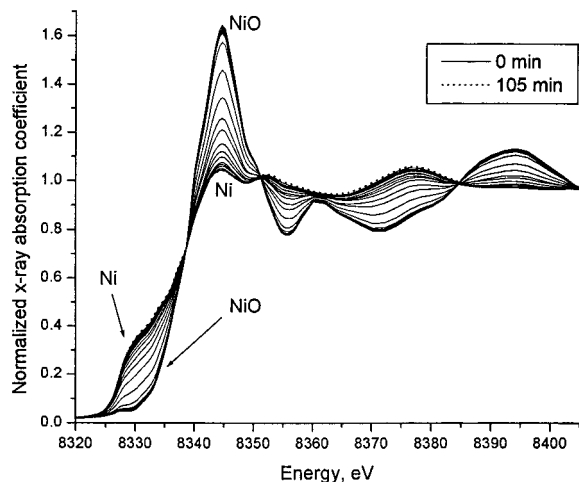
Figure 8. Time-resolved edge-step-normalized NEXAFS data for the reduction of NiO at 280 °C under a flow of hydrogen (~50 cm³/min). The data were aligned in absolute energy, using a reference Ni foil for energy calibration.

Figure 9. Fourier transform magnitudes of the time-resolved EXAFS data for the reduction of NiO at 260 °C. After addition of a phase shift correction of ~0.5 Å, unaccounted for in the figure, the peak positions at ~1.5, 2, and 2.5 Å become consistent with the presence of Ni–O (in NiO), Ni–Ni (in metal Ni), and Ni–Ni (in NiO) coordinations (see Table 1).

an amorphous NiO_x phase with special chemical properties. To address this issue, we studied the reduction of NiO powders with time-resolved NEXAFS/EXAFS. X-ray absorption is useful for examining possible changes in the electronic[19a,26] and local structural[19,33,34] properties of NiO during the reduction process. The coordination environments around Ni in the NiO and Ni phases are strikingly different (Table 1),[59,60] as are their electronic properties (the oxidation state changes from Ni^{2+} to Ni^0 upon reduction). Therefore, changes can be expected as well in the Ni *K*-edge absorption coefficient measured in situ during the NiO reduction.

NEXAFS data were collected at temperatures of 260, 280, and 300 °C. Since the reduction reaction is relatively fast at 280 and 300 °C, EXAFS measurements were done only at 260 °C. Our experiments showed marked time-dependent effects in both the NEXAFS (Figure 8) and EXAFS (Figure 9) data. In Figure 8, there is a monotonic decrease in the intensity of the Ni *K*-edge features for NiO, while the edge features for metallic Ni appear. After addition of a phase shift correction of ~0.5 D to the data in Figure 9, the peak positions at ~1.5, 2.0, and 2.5 Å become consistent with the presence of Ni–O (in Ni–O), Ni–Ni (in metal Ni), and Ni–Ni (in NiO) coordinations (see Table 1). These results point to a direct NiO→Ni transformation. Of course, on the basis of these figures alone, the presence of an intermediate NiO_x phase cannot be ruled out without a complete quantitative analysis of the data.

Although the theoretical methods of both EXAFS[62] and NEXAFS analyses are well developed[63] and the available data analysis programs are versatile enough to model the homoge-

neous systems during their phase transitions, the studies of heterogeneous mixtures have always been the bottleneck of the EXAFS analysis. One of the key reasons is the excessive number of theoretical variables, relative to the number of independent experimental data points, required to describe the superposition of the two or more different structural models. Another complication is that the possible data analysis procedures would be quite different whether it is assumed that the intermediate NiO_x phase is present or not, in addition to the coexisting NiO and Ni phases. This introduces an undesired model dependence in the results of the analysis.

The phase speciation problem of the XAFS data may be addressed from a quite different perspective, by using the principal component analysis (PCA).[64,65] In this work, we used a Mathematica-based program[66] implementing the PCA method to analyze the NEXAFS (for all the three reaction temperatures) and EXAFS (for the 260 °C) data and find out, model-independently, how many different species are present in the sample. For all the *M* spectra measured during the reaction studies (*M* varied from 14 to 50, for different samples and reaction temperatures), which were treated as vectors in an *L*-dimensional space (*L* is the number of energy points in each spectrum, *L* = 120 for the NEXAFS and 620 for the EXAFS data), the program obtained the corresponding sets of *M* eigenvalues and *M* eigenvectors (components). By examining the decay of the eigenvalues with the component number, we obtained the least number of components (i.e., species in the sample) sufficient to reproduce all the data using the "scree test".[65] This analysis showed overwhelmingly that two components (phases) are sufficient to adequately reproduce all the NEXAFS/EXAFS data. An example of such a reproduction of all the XANES data by just two components is shown in Figure 10. We would like to point out that the PCA method involves no structural modeling and, thus, is not biased toward any specific scenario of structural transformation. It obtains the number of species mixed together in the samples but does not

(62) Rehr, J. J.; Albers, R. C. *Rev. Mod. Phys.* **2000**, *72*, 621.
(63) Ankudinov, A. L.; Ravel, B.; Rehr, J. J.; Conradson, S. D. *Phys. Rev. B* **1998**, *58*, 7565.

(64) Frenkel, A. I.; Kleifeld, O.; Wasserman, S. R.; Sagi, I., unpublished.
(65) Wasserman, S. R. *J. Phys. IV* **1997**, *7*, C2−203.
(66) The PCA software was written by and is available from S. R. Wasserman.
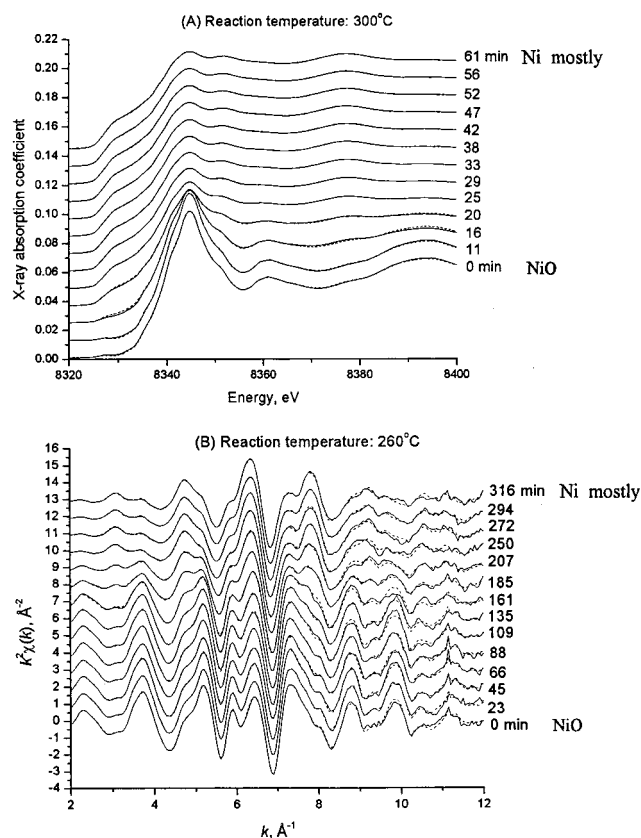
Figure 10. (A) NEXAFS data measured at 300 °C, together with their reproduction using the two principal components. (B) EXAFS data measured at 260 °C and their reproduction using the two principal components. The curves in (A) and (B) were shifted vertically for clarity.
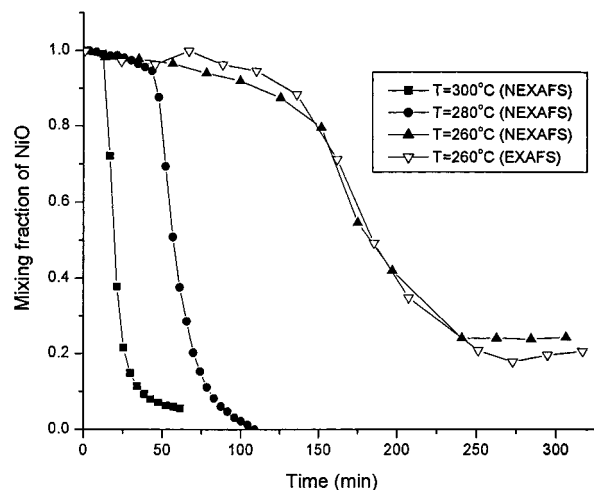
Figure 11. Mixing fraction of NiO as a function of time for reduction at 260, 280, and 300 °C, as obtained from the NEXAFS and EXAFS data by the principal component analysis. The powder samples were under a flow of H_2 (~50 cm³/min).

specify the identities of the species. However, because both the initial (NiO) and the final (Ni) phases should be present in the samples as individual species, *there is no room for the intermediate phase*, as our PCA results showed (otherwise, the

number of principal components would have to be three, in violation of the PCA results).

After establishing the number of species, their identities were then verified by a linear fit of the two principal components to the reference Ni and NiO experimental spectra at the same temperatures. The time-dependent mixing fractions of NiO were then obtained (see Figure 11). Remarkably, the mixing fractions obtained for the 260 °C reaction independently from NEXAFS and EXAFS agree with each other very well, emphasizing the reliability of the approach used here. Although the conditions and techniques in the experiments of Figures 6 and 11 are not the same, *clearly there is an induction period for the reduction of NiO powder in the NEXAFS/EXAFS results and in the XRD data*. During the induction time, O vacancies and active sites for the dissociation of H_2 are generated, but no significant amount of a new NiO_x phase is formed.

IV. Conclusions

In experiments with a NiO(100) crystal and NiO powders, oxide reduction is observed at atmospheric pressures and elevated temperatures (250−350 °C), but only after an induction period. The results of in situ time-resolved XRD and NEXAFS/EXAFS show a direct NiO→Ni transformation without accumulation of any intermediate phase. During the induction period, surface defect sites are created with a high efficiency for the dissociation of H_2. A perfect NiO(100) surface, the most common face of nickel oxide, exhibits a negligible reactivity toward H_2. The presence of O vacancies leads to an increase in the adsorption energy of H_2 and substantially lowers the energy barrier associated with the cleavage of the H−H bond. At the same time, adsorbed hydrogen can induce the migration of O vacancies from the bulk to the surface of the oxide. A correlation was observed between the concentration of vacancies in the NiO lattice and the rate of oxide reduction. These results illustrate the critical role played by O vacancies in the mechanism for reduction of an oxide. The kinetic models commonly used to explain the existence of an induction time during the reduction process can be important, but a more relevant aspect is the initial production of active sites for the rapid dissociation of H_2. The removal of O from the bulk or the nucleation of the metal phase becomes a rate-limiting factor only when enough H is available on the oxide surface.